JACS
JOURNAL OF THE AMERICAN CHEMICAL SOCIETY

Article

pubs.acs.org/JACS

Calcium Ion Gradients Modulate the Zinc Affinity and Antibacterial Activity of Human Calprotectin

Megan Brunjes Brophy, Joshua A. Hayden, and Elizabeth M. Nolan*

Department of Chemistry, Massachusetts Institute of Technology, Cambridge, Massachusetts 02139, United States

Supporting Information

ABSTRACT: Calprotectin (CP) is an antimicrobial protein produced and released by neutrophils that inhibits the growth of pathogenic microorganisms by sequestering essential metal nutrients in the extracellular space. In this work, spectroscopic and thermodynamic metal-binding studies are presented to delineate the zinc-binding properties of CP. Unique optical absorption and EPR spectroscopic signatures for the interfacial His_3Asp and His_4 sites of human calprotectin are identified by using Co(II) as a spectroscopic probe. Zinc competition titrations employing chromophoric Zn(II) indicators provide a 2:1 Zn(II):CP stoichiometry, confirm that the His_3Asp and His_4 sites of CP coordinate Zn(II), and reveal that the Zn(II) affinity of both sites is calcium-dependent. The calcium-insensitive Zn(II) competitor ZP4 affords dissociation constants of K_{d1} = 133 ± 58 pM and K_{d2} = 185 ± 219 nM for CP in the absence of Ca(II). These values decrease to $K_{d1} \leq 10$ pM and $K_{d2} \leq 240$ pM in the presence of excess Ca(II). The K_{d1} and K_{d2} values are assigned to the His_3Asp and His_4 sites, respectively. *In vitro* antibacterial activity assays indicate that the metal-binding sites and Ca(II)-replete conditions are required for CP to inhibit the growth of both Gram-negative and -positive bacteria. Taken together, these data provide a working model whereby calprotectin responds to physiological Ca(II) gradients to become a potent Zn(II) chelator in the extracellular space.

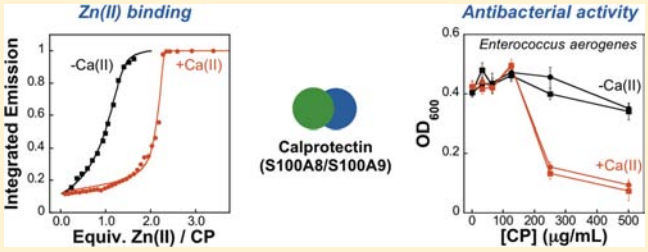

INTRODUCTION

Transition metal ions are essential nutrients for mammals as well as pathogenic microorganisms. Metal-ion withholding is therefore an important component of the innate immune response orchestrated by the host to inhibit colonization by invading bacteria and fungi, and to ensure that the host retains its own essential metal ions.[1−3] Iron sequestration by the mammalian antimicrobial proteins lactoferrin and siderocalin during infection is a canonical example of this innate immune mechanism.[4,5] In addition to iron, zinc is essential for all organisms,[6] and many pathogens also require manganese;[7] however, the details pertaining to the tug-of-war between host and pathogen for bioavailable zinc and manganese, including how the host precludes microbial uptake of these transition metal ions, are largely unknown.

Human calprotectin (CP) is one host-defense protein that prevents microbial colonization by scavenging manganese and zinc.[2,3,8,9] CP is a heterodimer or -tetramer of S100A8 (10.8 kDa, α subunit) and S100A9 (13.2 kDa, β subunit), two calcium-binding proteins of the S100 family.[10−14] White blood cells and epithelial cells express CP in either a constitutive (e.g., neutrophils) or an inducible (e.g., keratinocytes) manner. Remarkably, CP constitutes up to ∼40% of total cytoplasmic protein in neutrophils. These white blood cells migrate to sites of infection and combat invading pathogens on a short time-scale by producing reactive oxygen species and releasing an assortment of antimicrobial peptides and proteins that includes defensins, siderocalin, lysozyme, and CP into the extracellular space.[3,15] At sites of infection, the extracellular concentrations of CP reach >500 μg/mL (Figure 1A).[16] CP is an antifungal component of neutrophil extracellular traps (NETs),[17−20] and exhibits antibacterial activity against many Gram-positive and -negative human pathogens including *Staphylococcus aureus*,[9] *Salmonella enterica* serovar Typhimurium,[21] *Klebsiella* spp.,[22] *Listeria monocytogenes*,[23] and *Borrelia burgdorferi*.[24] CP prevents *S. aureus* colonization in murine tissue abscesses by sequestering manganese,[9] and it inhibits manganese-dependent superoxide dismutase in *S. aureus*, enhancing the susceptibility of this pathogen to oxidative stress.[25] Seminal investigations by other groups established that CP confers the zinc-reversible antifungal activity of neutrophil lysates and abscess fluid.[8,26,27] Later studies employing recombinant proteins confirmed that the CP hetero-oligomer is important because neither S100A8 nor S100A9 alone provided antifungal activity.[28] Recent investigations established that *Salmonella typhimurium* overcomes CP and competes with the commensal microbiota in the murine gut by expressing the high-affinity zinc uptake system ZnuABC.[21]

These studies motivate further investigations of the downstream physiological and pathological ramifications of transition metal sequestration by CP on microbial pathogens.[2,29] Equally important is evaluation of the consequences of metal chelation for the host during infection and under other physiological

Received: August 10, 2012
Published: October 19, 2012

   dx.doi.org/10.1021/ja307974e | J. Am. Chem. Soc. 2012, 134, 18089−18100

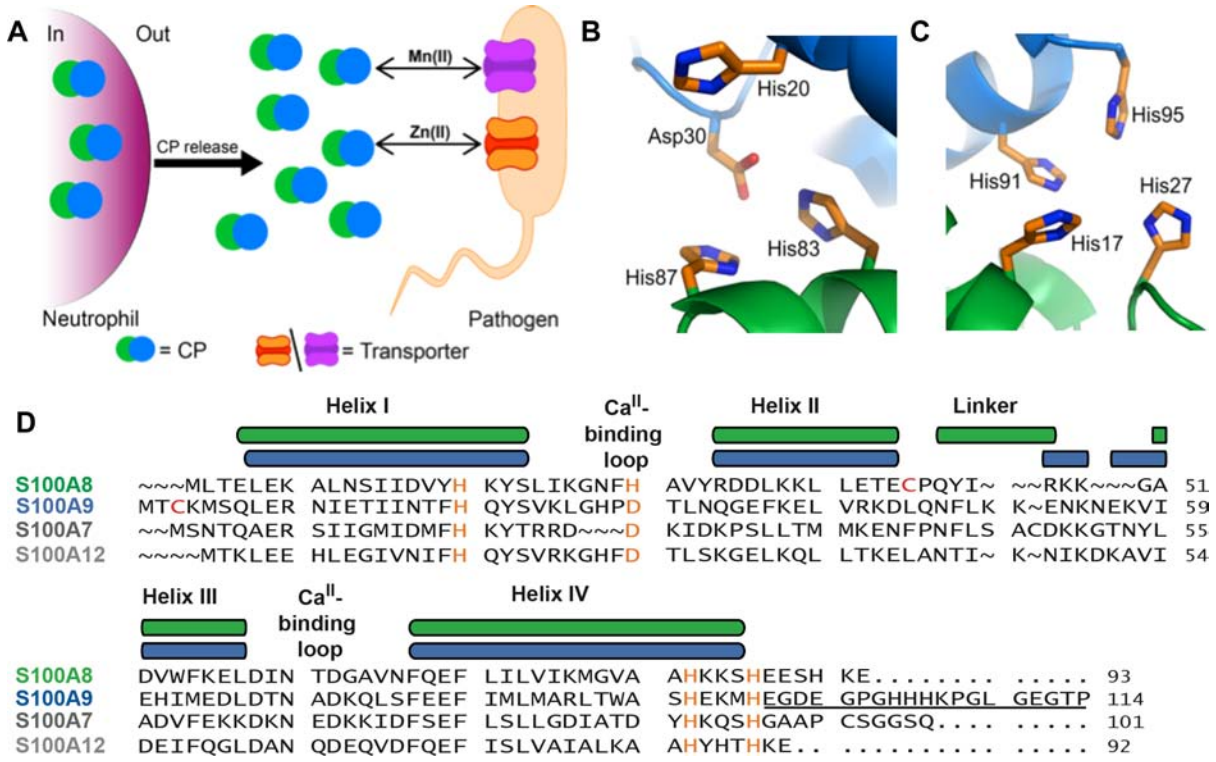

Figure 1. Proposed antimicrobial mechanism and structural features of human CP. (A) Proposed mechanism of action. CP is released from the neutrophil into the extracellular milieu where it competes with bacterial metal-ion transporters for bioavailable zinc and manganese. (B,C) The two putative transition metal-binding sites of human CP revealed at the dimer interface by X-ray crystallography (PDB: 1XK4). S100A8 is colored green and S100A9 is colored blue, and the putative metal-binding residues are shown in orange. Panel B illustrates the His_3Asp site (site 1), and panel C depicts the His_4 site (site 2). See ref 37 and Figure S1 of Supporting Information for the complete structure. (D) Amino acid alignment of the human calprotectin subunits S100A8 and S100A9 with human S100A7 and human S100A12. Alpha helices I–IV, the calcium-binding loops, and linker regions of S100A8 and S100A9 are color-coded and depicted above the alignments. The disordered C-terminus of S100A9 is underlined. The identified (A7, A12) and putative (A8, A9) metal-binding residues are highlighted in orange. The cysteine residues of S100A8 and S100A9 that were mutated to serine in this work are colored in red. Both S100A7 and S100A12 form homodimers, coordinate transition metals by interfacial His_3Asp motifs, and are involved in the innate immune response.

circumstances. Links between CP and zinc have been identified for human pathologies that include inflammation and cancer,[30,31] amyloid formation in the aging prostate,[32] and erroneous zinc metabolism.[33,34] Molecular-level understanding of how CP contributes to bacterial and mammalian physiology in broad terms requires elucidation of both its metal-binding properties and the biological significance of the metal-bound forms. Motivated by the multiple links between CP and Zn(II) in the host/pathogen interaction and human disease, we focus on the zinc-binding properties of CP in this work.

The coordination chemistry of CP is largely unexplored. Like other S100 proteins,[35,36] each CP subunit contains two Ca(II)-binding EF-hand domains with varying amino acid compositions (Figures 1 and S1, Supporting Information), and Ca(II) binding causes CP to oligomerize from a heterodimeric ($\alpha\beta$) to a heterotetrameric ($\alpha_2\beta_2$) form.[12−14] The only available CP X-ray crystal structure is for the human protein in a heterotetrameric form.[37] This structure serves as a guide and reveals two putative transition metal-ion binding sites at each A8/A9 dimer interface (Figures 1B,C and S1). S100A8 and S100A9 each contribute two residues to each site. Site 1 contains a His_3Asp motif formed by A8(H83), A8(H87), A9(H20), and A9(D30). These same amino acids comprise the metal-binding sites of other S100 proteins (e.g., S100A7,[38] S100A12[39]) and also the primary coordination spheres of various metalloenzymes such as zinc metalloproteinases and manganese/iron superoxide dismutases. Site 2 displays a His_4 motif formed by A8(H17), A8(H27), A9(H91), and A9(H95). The amino acid sequence alignment presented in Figure 1D demonstrates that the His_4 motif arises from His27 of S100A8, and that several Glu/Asp residues of S100A9 are in its vicinity. The His_4 composition of this putative metal-binding site is rare for S100 proteins and metalloproteins as a whole (*vide infra*). S100A9 exhibits an unusual C-terminal extension (Figure 1D), which is disordered in the crystal structure and houses a number of potential metal-coordinating residues (His, Asp, Glu). CP therefore presents a complex and intriguing bioinorganic coordination chemistry problem that involves multiple types of potential binding sites and divalent cations, and requires careful examination. Toward understanding zinc binding by CP, isothermal titration calorimetry (ITC) studies of human CP and a mutant protein lacking the eight residues forming sites 1 and 2 (His→Asn and Asp→Ser mutations, hereafter ΔZn/Mn) were reported recently.[25] An exothermic event was observed upon zinc addition to the wild-type protein, indicating zinc complexation, whereas negligible enthalpy change occurred for the mutant protein. This study suggested that sites 1 and 2 are important for high-affinity Zn(II) binding (*vide infra*); however, the precise site(s) of Zn(II) coordination, the details of the coordination environment(s), and whether calcium plays a role in Zn(II) complexation, remain unclear.

dx.doi.org/10.1021/ja307974e | J. Am. Chem. Soc. 2012, 134, 18089−18100

Herein we report detailed solution spectroscopic and thermodynamic investigations designed to delineate the zinc-binding properties of human CP and to elucidate whether calcium plays a role in zinc complexation. These studies provide spectroscopic signatures and unambiguous determination of the high affinity zinc-binding sites, in addition to rigorous investigations of Zn(II) complexation to CP under low and high calcium concentrations. This work reveals that calprotectin strategically employs physiological calcium gradients to tune its zinc affinity. We propose a model whereby CP exists in its lower zinc affinity form in the neutrophil cytoplasm and, following release, binds calcium and morphs into a potent Zn(II) chelator with antimicrobial activity in the extracellular space.

EXPERIMENTAL SECTION

Materials and General Methods. All solvents, reagents, and chemicals were obtained from commercial suppliers and used as received unless noted otherwise. FluoZin-3 (FZ3) and Mag-Fura-2 (MF2) were purchased from Invitrogen and Zinpyr-4 (ZP4) from Strem Chemicals, Inc. Zincon monosodium salt was obtained from Alfa Aesar. Oligonucleotide primers were synthesized by Integrated DNA Technologies, Inc. (Coralville, IA) and used as received (standard desalting protocol). A Biorad MyCycler thermocycler was employed for all polymerase chain reactions (PCR). Chemically competent *E. coli* TOP10 and BL21 (DE3) cells were prepared in-house by standard protocols. An illustra GFX PCR DNA and Gel Band Purification Kit (GE Healthcare) was utilized for purifying all PCR products, and a Qiagen miniprep kit was employed for all plasmid isolations. DNA sequencing was performed by staff members at the MIT Biopolymers facility. All buffers, aqueous solutions, and oligonucleotide stock solutions were prepared using Milli-Q water (18.2 MΩ, 0.22 μm filter). Milli-Q water was also used to prepare Luria Broth (LB), LB agar plates, and Tryptic Soy Broth (TSB). An Agilent 8453 diode array spectrophotometer was employed for monitoring OD_{600} values of bacterial cultures unless noted otherwise. Protein concentrations were routinely quantified by using a calculated extinction coefficient for the CP heterodimer (ε_{280} = 18 450 M^{-1} cm^{-1}, Table S5, Supporting Information), and the absorption readings were taken with either a BioTek Synergy HT plate reader outfitted with a calibrated Take3 Micro-Volume plate or an Agilent 8453 diode array spectrophotometer using a 1-cm path length quartz cuvette (Starna). All CP concentrations are in terms of the CP heterodimer ($\alpha\beta$). All reported stoichiometries are per CP heterodimer ($\alpha\beta$). Experimental procedures for protein mass spectrometry, analytical size exclusion chromatography (SEC), and circular dichroism spectroscopy are provided as Supporting Information. Tables S1−S6 of Supporting Information contain primers and primer pairings employed for cloning and site-directed mutagenesis, protein nomenclature, and the molecular weights and calculated extinction coefficients of CP and all mutant proteins.

Cloning, Mutagenesis, Overexpression, and Purification of CP and Mutants. Synthetic genes containing the *E. coli* optimized nucleotide sequences for human S100A8 and S100A9 were obtained in the pJ201 vector from DNA 2.0 and subcloned into the *Nde*I and *Xho*I sites of pET41a (Supporting Information). A modified Quick-Change site-directed mutagenesis protocol (Stratagene) was employed to generate the CP mutants. The resulting pET41a-*S100A8* and pET41a-*S100A9* expression plasmids were transformed into chemically competent *E. coli* BL21(DE3) cells. Cultures from single colonies were grown to saturation in LB media containing 50 μg/mL kanamycin (37 °C with agitation, $t \approx 16$ h), and freezer stocks were prepared by diluting the overnight cultures with an equal volume of 1:1 water/glycerol (sterile) and stored at −80 °C. For protein overexpression, overnight cultures were grown to saturation in LB media containing 50 μg/mL kanamycin (37 °C, 150 or 175 rpm, $t \approx$ 16 h) and diluted 1:100 into fresh LB media containing 50 μg/mL kanamycin, incubated at 37 °C with shaking at 150 rpm, and induced with 500 μM IPTG at $OD_{600} \approx 0.6$. The cultures were incubated at 37 °C for an additional 3−4 h ($OD_{600} \approx 1.5$), and pelleted by centrifugation (4200 rpm × 30 min, 4 °C). The cell pellets were transferred to preweighed 50-mL polypropylene centrifuge tubes, flash frozen in liquid N_2, and stored at −80 °C. The reconstitution and purification of heterodimeric CP and all mutants were performed by making several modifications to literature procedures.[10,25,37] Complete details for cloning, site-directed mutagenesis, protein overexpression and purification, protein storage, and handling are provided as Supporting Information.

General Methods for Optical Absorption and Fluorescence Spectroscopic Measurements. All precautions were taken to minimize metal−buffer equilibria and metal ion contaminations. Non-coordinating buffers were employed for metal-binding studies and dissociation constant determination to prevent complications resulting from metal−buffer equilibria. Aqueous solutions were prepared with fresh Milli-Q water (18.2 MΩ, 0.22-μm filter). Metal-free TraceSELECT (99.999%) NaCl was purchased from Sigma-Aldrich, and metal-free ULTROL grade HEPES (free-acid) was obtained from Calbiochem. To minimize metal-ion contamination, only Teflon-coated spatulas were employed to transfer all buffer reagents, and the solutions were treated with 10 g/L Chelex by stirring in a polypropylene beaker for at least 1 h before use. Prior to use, the Chelex resin was removed by filtering the mixture through a 0.22-μm filter (Corning) or by centrifugation. Some fluorescent sensors detected Ca(II) contamination from the 0.22-μm filters, and centrifugation was always employed for removing Chelex from buffers employed for fluorescence spectroscopy. The buffers were stored in sterile polypropylene tubes. Protein aliquots were thawed on ice, and the storage buffer was exchanged (at least three 5× dilutions) by using a 0.5-mL Amicon centrifugal filter device with a 10-kDa MWCO membrane (Millipore). Cobalt stock solutions were prepared from 99.999% $CoCl_2$ hydrate (Sigma Aldrich) and Milli-Q water. All zinc stock solutions were prepared from 99.999% anhydrous $ZnCl_2$ (Sigma Aldrich) and Milli-Q water. All Co(II)-binding studies were conducted at pH 7.0 in 75 mM HEPES, 100 mM NaCl buffer. The Co(II) studies were conducted at pH 7.0 because CP-Ser (400 μM, *vide infra*) precipitated following addition of Co(II) at pH 7.5. With the exception of the Co(II) displacement experiments, all Zn(II)-binding studies were conducted at pH 7.5 in 75 mM HEPES, 100 mM NaCl buffer. DMSO stock solutions of approximately 1 mM ZP4 were prepared, partitioned into 50-μL aliquots, stored at −20 °C, and thawed immediately before use. Stock solutions of FZ3 and MF2 were prepared in Milli-Q water, partitioned into aliquots, and stored at −20 °C. These metal- and light-sensitive chromophores were covered in aluminum foil, thawed immediately before use, and handled in the dark. Stock solutions of Zincon in DMSO were prepared immediately before use and kept covered in aluminum foil. Optical absorption spectra were collected on a Beckman Coulter DU 800 spectrophotometer thermostatted at 25 °C with a Peltier temperature controller or an Agilent 8453 diode-array spectrophotometer controlled with manufacturer-supplied software and thermostatted at 25 °C by a circulating water bath. Quartz cuvettes with 1-cm path lengths (Starna) were employed for all optical absorption measurements. All optical absorption and fluorescence spectroscopic measurements were performed at least two times, and all titrations were performed at least in triplicate. Fluorescence spectra were collected on a Photon Technologies International QuantaMaster 40 fluorimeter outfitted with a continuous xenon source for excitation, autocalibrated QuadraScopic monochromators, a multimode PMT detector, and a circulating water bath maintained at 25 °C. This instrument was controlled by the FelixGX software package. FelixGX was routinely employed to integrate the emission spectra.

Electron Paramagnetic Resonance Spectroscopy. Low-temperature EPR spectra (X-band, 9 GHz) were recorded on a Bruker EMX spectrometer equipped with an ER 4199HS cavity and an Oxford Instruments ESR900 continuous flow liquid helium cryostat. Low-temperature EPR samples were housed in 4-mm (outer diameter) quartz EPR tubes and frozen in liquid nitrogen prior to analysis. The temperature was monitored with either a Cernox sensor or a

thermocouple. A copper-EDTA spin standard was used to account for all relevant intensity factors. All samples were measured under nonsaturating and saturating conditions. All cobalt spectra were recorded at 9.38 GHz and analyzed with SpinCount, which is available from Prof. Michael Hendrich at Carnegie Mellon University.

Zinc Stoichiometry Determination. In one set of experiments, a 2-mL solution containing ca. 10 μM CP or mutant and 25 μM Zincon (75 mM HEPES, 100 mM NaCl, pH 7.5) was titrated with Zn(II). The absorbance change at 621 nm was recorded and plotted against the total concentration of Zn(II). In a second set of experiments, an approximately equimolar mixture of CP and MF2 (ca. 10 μM each) was prepared and titrated with Zn(II) (2 mL volume; 75 mM HEPES, 100 mM NaCl, pH 7.5). After each Zn(II) addition, the resulting mixture was incubated at room temperature for 15 min, and the optical absorption spectrum was recorded. The absorbance increase at 325 nm and decrease at 366 nm were recorded and plotted against total Zn(II). The Zn(II) stock solutions were prepared by volumetric dilution of a 100 mM stock solution prepared from $ZnCl_2$ and water and the resulting concentrations verified by using 4-(2-pyridylazo)-resorcinol (PAR, $\varepsilon_{500} \approx 80\,000$ M^{-1} cm^{-1} for the 1:2 complex at pH 7.3) obtained from Acros Organics. To determine whether Ca(II) influences the Zn:CP stoichiometry, the Zincon experiment was repeated in the presence of 200 μM Ca(II). Zincon has reported Zn(II) K_d values of 12.6 and 5.8 μM.[40,41] Reported Zn(II) K_d values of MF-2 are 20 and 36 nM.[42,43]

Zinc Affinity Determination with FZ3. Solutions containing ca. 2 μM FZ3 and ca. 10 μM CP were prepared at pH 7.5 (75 mM HEPES, 100 mM NaCl), and the emission spectrum was recorded from 500 to 650 nm (λ_{ex} = 493 nm). An aliquot of Zn(II) from a freshly prepared 2 mM solution was added, and the solution was mixed in the cuvette and the resulting emission spectrum recorded. The emission was integrated from 500 to 650 nm by using the KaleidaGraph software package.

Zinc Affinity Determination with ZP4. Competition titrations with CP and ZP4 were employed to determine the dissociation constants of CP for Zn(II). In a typical experiment, an aliquot from a ~1 mM DMSO stock solution of ZP4 was diluted to a final concentration of ~2 μM in a total volume of 2 mL (75 mM HEPES, 100 mM NaCl, pH 7.5). After the optical absorption (ε_{506} = 61 000 M^{-1} cm^{-1})[44] and emission spectra of this solution were recorded, an aliquot of CP was added to provide a final concentration of ~5 or ~10 μM as indicated, and the optical absorption and emission spectra were recorded again. The absorption and fluorescence spectra of ZP4 were unperturbed by the addition of CP. This CP/ZP4 mixture was titrated with Zn(II) using a freshly prepared working solution from a 100 mM stock of $ZnCl_2$ in water that was quantified by PAR. After each Zn(II) addition, the solution was mixed gently and incubated in the dark for a minimum of 10 min. The emission spectrum was recorded from 505 to 650 nm (λ_{ex} = 495 nm), and the resulting spectra were integrated over this range. The integrated emission versus the concentration of Zn(II) added was plotted, and the resulting titration curve was fit to a two-site model using the DynaFit software and a custom script (Supporting Information). The dye response factors required by DynaFit were determined for free ZP4 in the presence of 100 μM EDTA and for ZP4 in the presence of 100 μM Zn(II) (75 mM HEPES, 100 mM NaCl, pH 7.5). For CP/ZP4 competition experiments in the presence of Ca(II), the same procedures were employed except that 100–450 μM Ca(II) was added to the buffer. The reported Zn(II) K_d values were obtained by averaging the K_d values obtained from fitting three independent titrations. The errors are the standard deviations from the mean.

Calcium-Dependent Zn(II) Sequestration by CP. A solution of CP/ZP4 (75 mM HEPES, 100 mM NaCl, pH 7.5) was first titrated with Zn(II) to afford maximum ZP4 turn-on, and an aliquot of Ca(II) from a 100 mM stock solution was added to provide a final Ca(II) concentration of 200 μM. The resulting changes in ZP4 emission were monitored over the course of 300 min. Once the emission intensity returned to the baseline (apo ZP4) value, the solution was titrated with Zn(II) until maximum emission from the Zn:ZP4 complex was restored. The maximal ZP4 emissions achieved before and after Ca(II) addition were in excellent agreement, confirming the integrity of the ZP4 sensor over the course of the experiment.

To probe Zn(II) dissociation from CP ($\alpha_2\beta_2$), a solution containing ~6 μM CP, ~3 μM Zn(II), and 200 μM Ca(II) was incubated at room temperature for 30 min, and an aliquot of ZP4 was added to provide a final concentration of 2 μM (75 mM HEPES, 100 mM NaCl, pH 7.5). The ZP4 emission was monitored over 300 min. Controls without CP and without Zn(II) were conducted in parallel. With the exception of the no CP control, which exhibited full ZP4 turn-on, addition of 50 μM Zn(II) to the samples after the incubation period resulted in full ZP4 turn-on, verifying the integrity of ZP4 over the course of the experiment.

Antimicrobial Activity Assays. All bacterial strains were purchased from ATCC. To first confirm that recombinant wild-type CP exhibited antibacterial activity, the ability of CP to inhibit the growth of *S. aureus* ATCC 25923 was monitored by using a modified literature protocol.[25] *S. aureus* ATCC 25923 was grown overnight with shaking (37 °C, 16 h) in 6 mL of TSB without dextrose. The overnight culture was diluted 1:100 into 6 mL of fresh TSB without dextrose and grown for ~2 h at 37 °C until the OD_{600} reached ~0.6. The culture was diluted 1:500 in two steps (1:100 and then 1:5) into antimicrobial assay (AMA) media (62:38 ratio of 20 mM Tris-HCl pH 7.5, 100 mM NaCl, 5 mM BME with or without 3 mM $CaCl_2$, and TSB) and used immediately. Protein aliquots were thawed on ice, diluted 10-fold with AMA buffer (20 mM Tris-HCl pH 7.5, 100 mM NaCl, 5 mM BME), and buffer exchanged three times using a 10-kDa cutoff 0.5-mL Amicon microcentrifuge tube (Millipore). The resulting protein concentrations were determined, and the aliquots diluted with AMA media to provide 10× protein stocks (5000 μg/mL to 312.5 μg/mL). The antibacterial activity assays were performed in polystyrene 96-well plates (Corning). Each well contained a 90-μL aliquot of the diluted bacterial culture and a 10-μL aliquot of the 10× protein stock solution or no-protein control. Each well condition was prepared in triplicate. Each plate was wrapped with parafilm and incubated at 37 °C with shaking at 150 rpm in a tabletop incubator shaker housing a beaker of water. The OD_{600} values were measured at varying time points (0–24 h) by using a plate reader. This assay was also performed with CP-Ser. For assays conducted with Ca(II)-supplemented media, the final concentration of Ca(II) resulting from the supplement was 2 mM.

To investigate the antibacterial activity of CP and CP-Ser against *Escherichia coli* ATCC 25922 and *Enterobacter aerogenes* ATCC 13048, growth inhibitory assays were conducted as described above with the following modifications: (i) the TSB contained dextrose, (ii) the assays were conducted at 30 °C, (iii) the OD_{600} values were recorded after 24 h incubation, and (iv) no beaker of water was housed in the incubator shaker. These assays were also conducted in the absence and presence of the 2 mM Ca(II) supplement.

To ascertain the effect of supplementing AMA assay media with CP, CP-Ser, ΔHis_3Asp, ΔHis_4, or $\Delta\Delta$ on the growth of a variety of bacterial species, a series of assays were conducted as described above for *S. aureus* ATCC 25923 except that (i) the assays were conducted at 30 °C, (ii) a single protein concentration of 500 μg/mL was employed, and (iii) the OD_{600} was monitored at t = 8 and 20 h. *S. aureus* ATCC 25923, *E. coli* ATCC 25922, and *E. aerogenes* ATCC 13048 were investigated.

For all antibacterial activity assays, each experiment was repeated a minimum of three times and with at least two independent single-colony cell stocks of each bacterial species.

RESULTS

Design, Preparation, and Characterization of a Calprotectin Mutant Family. A mutant family was designed for elucidating the transition metal-ion binding sites of CP. Amino acids comprising the putative His_4 (His17 and His27 of A8; His91 and His95 of A9) and His_3Asp (His83 and His87 of A8; His20 and D30 of A9) coordination sites were systematically replaced with non-coordinating alanine by using site-directed mutagenesis. Mutant proteins containing either a

dx.doi.org/10.1021/ja307974e | J. Am. Chem. Soc. 2012, 134, 18089–18100

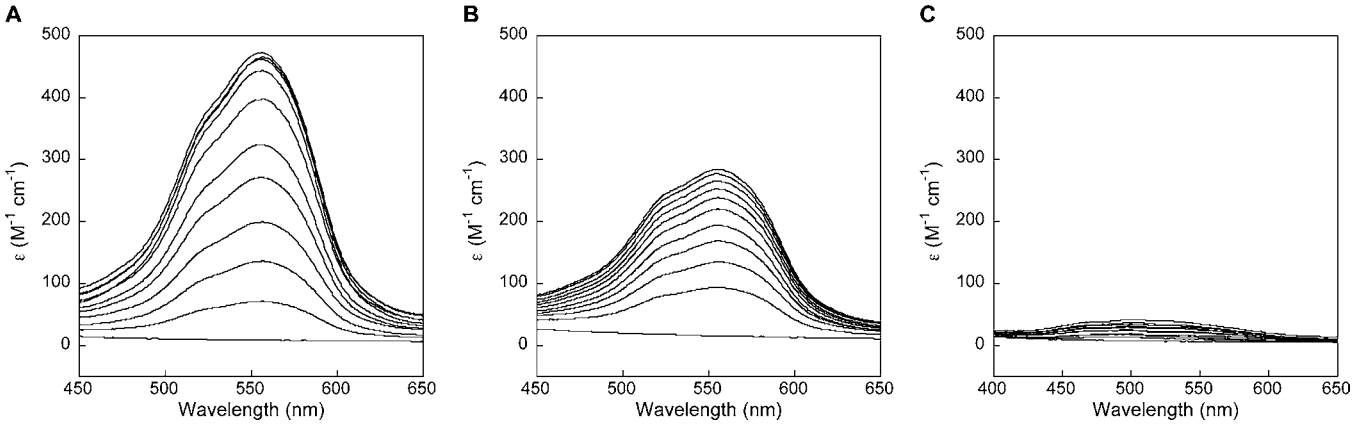

Figure 2. Cobalt binding to CP monitored by optical absorption spectroscopy. CP (400 μM) was titrated with 0−5 equiv of Co(II) at pH 7.0 (75 mM HEPES, 100 mM NaCl) and 25 °C. (A) Titration of CP-Ser with Co(II). A d−d transition centered at 556 nm (ε = 480 M^{-1} cm^{-1}) is observed. (B) Titration of CP-Ser ΔHis_4 with Co(II). A d−d transition centered at 556 nm (ε = 280 M^{-1} cm^{-1}) is observed. (C) Titration of CP-Ser ΔHis_3Asp with Co(II). A d−d transition centered at 499 nm (ε = 38 M^{-1} cm^{-1}) is observed, and an expanded version of the plot is given in Figure S29. These titrations indicate that Co(II) binds to both the His_3Asp and His_4 sites of CP.

single point mutant, two mutations in the His_3Asp (D30A/H83A) or His_4 (H27A/H91A) sites, or deleted sites (ΔHis_3Asp, ΔHis_4, and $\Delta\Delta$, the latter of which has neither binding site) were purified and characterized (see Figures S2 and S3 and Tables S2−S5). For the metal-binding studies, Cys42 of S100A8 and Cys3 of S100A9 were also mutated to Ser residues (hereafter CP-Ser) to avoid using high concentrations of reducing agents such as dithiothreitol and β-mercaptoethanol. Each of these reagents has an affinity for Zn(II) and will compromise any metal-binding experiments. For protein isolation and purification, *E. coli*-optimized synthetic genes for wild-type S100A8 and S100A9 were ligated into the *Nde*I and *Xho*I sites of pET41a and each of the S100A8/S100A9 subunits were overexpressed separately in *E. coli* BL21(DE3) cells. The CP heterodimer was obtained from a denaturing and refolding protocol modified from the literature,[10,37] purified by ion exchange and size exclusion chromatographies, and dialyzed against Chelex resin prior to storage (10 g/L; 20 mM HEPES, 100 mM NaCl, pH 8.0). Yields of the CP-Ser heterodimers varied from approximately 10 mg/2L culture ($\Delta\Delta$) to 45 mg/2L culture (CP-Ser), and the purified wild-type protein was obtained in yields of 80 mg/2L. Each protein was characterized by SDS-PAGE, ESI mass spectrometry, circular dichroism (CD) spectroscopy, and analytical size exclusion chromatography (SEC). SDS-PAGE analysis revealed that all CP proteins were obtained in high purity (Figures S2 and S3), and ESI-MS confirmed the expected masses for the two subunits of each protein (Table S7). The CD spectra were in excellent agreement with literature spectra[10] of wild-type CP with local minima at 208 and 222 nm, confirming α-helical secondary structure that is largely unperturbed by Ca(II) addition (Figures S4−S11). Analytical SEC established that each protein was isolated as the $\alpha\beta$ heterodimer. Purified wild-type and all mutant CPs eluted at ca. 10.8 mL, corresponding to a molecular weight of ca. 36 kDa and assigned to the 24-kDa heterodimer (Figures S12−S26 and Table S8). Addition of 2 mM Ca(II) to the running buffer (20 mM HEPES, 100 mM NaCl, pH 8.0, Chelex-treated) resulted in disappearance of the 10.8 mL peak and formation of a new peak at ca. 10.2 mL consistent with a molecular weight of 48 kDa for all protein samples, which confirmed Ca(II)-induced $\alpha_2\beta_2$ heterotetramer formation for all CP mutants. In some instances, small shoulders of lower elution volume were observed and attributed to higher-order oligomers. Titrations of 100 μM CP or CP-Ser with 0−8 equiv of Ca(II) were monitored by analytical SEC and resulted in a stepwise decrease in the 24-kDa peak and increase in the 48-kDa peak (Figure S27); however, complete formation of the $\alpha\beta$ heterotetramer was not observed, suggesting that either CP-bound Ca(II) was lost during the chromatography run, or 8 equiv of Ca(II) was insufficient to afford complete oligomerization to the heterotetrameric form. Either possibility may be attributed to, at least in part, the fact that both A8/A9 subunits house N-terminal noncanonical EF-hand domains expected to coordinate Ca(II) with relatively low affinities.[35] In total, these studies demonstrate that the various mutations incorporated into the CP scaffold do not compromise the overall protein fold or the ability of CP to undergo Ca(II)-dependent tetramerization.

Calcium Stabilizes the Calprotectin Protein Fold. Thermal denaturation of 10 μM CP-Ser ($\alpha\beta$) gave a melting temperature (T_m) of 59 °C at pH 8.5 (1 mM Tris, 0.5 mM EDTA). When 2 mM Ca(II) was added to CP-Ser, the denaturation curve shifted by 20 °C to provide a T_m of 79 °C (Figure S28). Calcium coordination and tetramerization of CP-Ser stabilizes the protein fold to thermal denaturation. This observation is in general agreement with the results obtained from differential scanning calorimetry investigations of wild-type CP isolated from granulocytes or produced recombinantly where an 11−13 °C increase in the transition temperature was observed with Ca(II) addition.[45]

Calprotectin Binds Co(II) at the His_3Asp and His_4 Sites of the Dimer Interface. High-spin Co(II) ($3d^7$) is a useful optical absorption spectroscopic probe for biological Zn(II) ($3d^{10}$) sites because of the well-established correlations between Co(II) ligand field transitions and coordination geometries.[46] Addition of 0−5 equiv of Co(II) to CP-Ser (400 μM, $\alpha\beta$) at pH 7.0 (75 mM HEPES, 100 mM NaCl) resulted in formation of a pink solution with a d−d transition centered at 556 nm (ε = 480 M^{-1} cm^{-1}) (Figure 2A). A similar absorption feature with a lower extinction coefficient (556 nm, ε = 280 M^{-1} cm^{-1}) was observed during titration of ΔHis_4 (400 μM, $\alpha\beta$) with Co(II), and a weak absorption feature centered at 499 nm (ε = 38 M^{-1} cm^{-1}) formed following

dx.doi.org/10.1021/ja307974e | J. Am. Chem. Soc. 2012, 134, 18089−18100

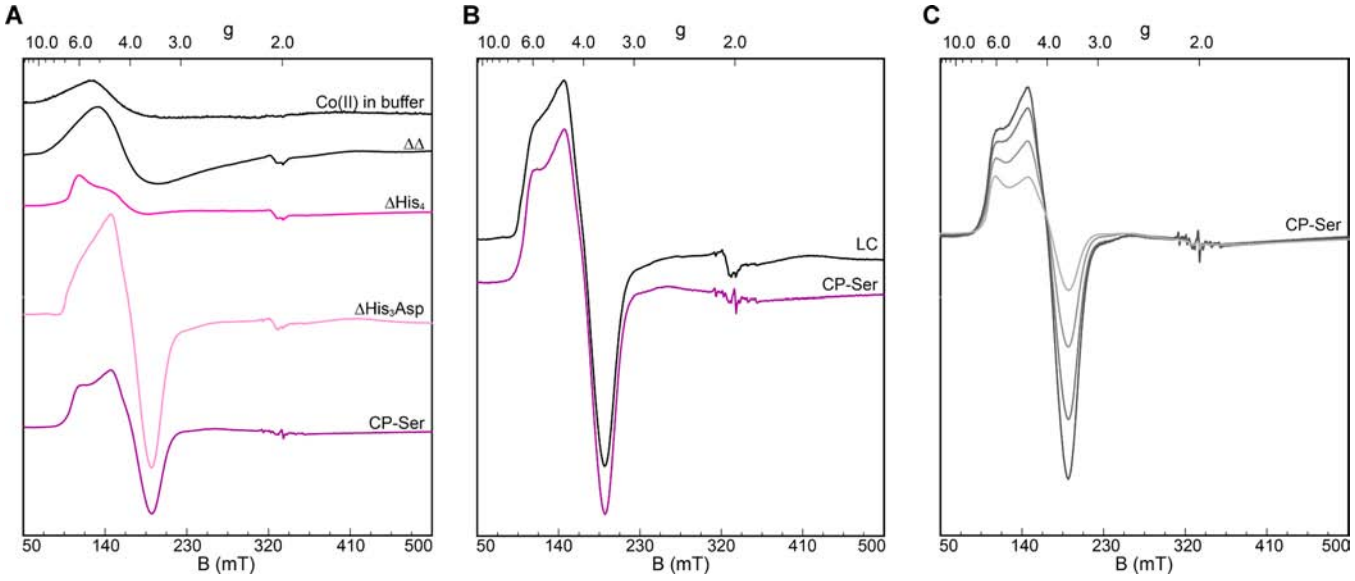

Figure 3. Low-temperature EPR spectroscopic signals of Co(II)-bound CP. (A) EPR spectra of 1.1 mM CP-Ser and the indicated metal-binding site mutants in the presence of 0.8 equiv of Co(II) at pH 7.0 (20 mM HEPES, 100 mM NaCl). The colors of the CP-Ser and ΔHis_4 spectra indicate the color of the samples following Co(II) addition. The samples of ΔHis_3Asp and $\Delta\Delta$, in addition to the Co(II) in buffer reference, were colorless. Instrument conditions: temperature, 10.6 K; microwave, 2 mW at 9.38 GHz; modulation amplitude, 8.0 G. (B) The black trace is a linear combination of the ΔHis_4 and ΔHis_3Asp spectra exhibited in panel A. Combination of $^1/_2$ ΔHis_4 and $^1/_2$ ΔHis_3Asp closely reproduces the spectrum of CP-Ser shown in purple. (C) Power saturation experiments. EPR spectra of the CP-Ser sample from panel A were recorded at 10.6 K with powers of 0.6, 2, 6, and 20 mW. The gray scale indicates increasing power from black to light gray.

titration of ΔHis_3Asp (400 μM, $\alpha\beta$) with Co(II) (Figures 2B,C and S29). The presence of 2 mM Ca(II) had negligible effect on the absorption spectrum of cobalt-bound CP-Ser (100 μM, Figure S30); however, introduction of Co(II) into Ca/CP mixtures caused precipitation at higher protein concentrations. The λ_{max} values and extinction coefficients for the CP mutants indicate that both sites 1 and 2 coordinate Co(II), and with different geometries. Indeed, protein-bound Co(II) in a tetrahedral environment coordinated by N- and O-donors typically exhibits $\varepsilon > 300$ M^{-1} cm^{-1}, whereas five- and six-coordinate Co(II) provide less intense transitions with $250 > \varepsilon > 50$ M^{-1} cm^{-1} and $\varepsilon < 50$ M^{-1} cm^{-1}, respectively.[46] Because of different ligand field stabilization energies, the λ_{max} values also vary with coordination number from 625 ± 50 nm (four-coordinate, tetrahedral) to 525 ± 50 nm (six-coordinate, octahedral).[46] Taking these trends into account, the optical absorption data for the CP mutants indicate Co(II) coordination in a four- or five-coordinate manner at the His_3Asp site, suggesting that the aspartate residue may be mono- or bidentate. The His_4 site likely provides a six-coordinate geometry, although a five-coordinate geometry cannot be ruled out. Unidentified water molecules, buffer components, or protein residues may contribute to the coordination sphere of this His_4 site.

Cobalt complexation by CP was further evaluated by EPR spectroscopy, which provided unambiguous support for two distinct Co(II)-binding sites (Figures 3 and S31). Addition of 0.8 equiv of Co(II) to CP-Ser (1.1 mM, $\alpha\beta$) at pH 7.0 (75 mM HEPES, 100 mM NaCl) gave rise to a broad EPR signal at 10.6 K typical of high-spin Co(II) ($S = 3/2$) with no observable ^{59}Co ($I = 7/2$) nuclear hyperfine structure (Figure 3A).[47,48] This signal contained absorption-like and derivative features at $g_{eff} = 6.04$ and 4.1, respectively. Unique EPR signals indicating protein-bound high-spin Co(II) for the ΔHis_4 and ΔHis_3Asp mutants prepared under the same conditions were observed and support different Co(II) coordination motifs. The ΔHis_3Asp Co(II) spectrum was characterized by a sharp derivative feature at $g_{eff} = 4.0$. The ΔHis_4 Co(II) spectrum exhibited a markedly less intense signal that contained both absorption and derivative features at $g_{eff} = 6.06$ and 4.14. All Co(II)/CP samples exhibited additional resonances at $g = 2.02$. Linear combinations the ΔHis_4 and ΔHis_3Asp spectra closely reproduced the CP-Ser spectrum (Figure 3B) and provided $\Delta His_4/\Delta His_3Asp$ ratios ranging from 1:2 to 2:1 depending on the sample. Addition of Co(II) to $\Delta\Delta$ resulted in a signal resembling the Co(II)/buffer standard, and this signal had a negligible impact on efforts to reproduce the CP-Ser signal through linear combinations. Moreover, power saturation of the CP-Ser EPR signal at 10.6 K revealed distinct saturation behavior in different regions of the spectrum (Figure 3C and S31), supporting the presence of multiple Co(II)-bound species.[47,49] These studies confirm Co(II) complexation at sites 1 and 2, and that both sites are occupied in the presence of substoichiometric Co(II).

The CD spectrum of 10 μM CP-Ser was unperturbed by the addition of 10 equiv of Co(II) in both the presence and absence of Ca(II), revealing that Co(II) binding has negligible impact on the overall secondary structure of CP (Figure S32).

Calprotectin Binds Zn(II) at the His_3Asp and His_4 Sites of the Dimer Interface. Addition of Zn(II) to a 1:1 mixture of CP-Ser ($\alpha\beta$, 100 μM) and Co(II) buffered at pH 7.0 (75 mM HEPES, 100 mM NaCl) resulted in a gradual decrease in the electronic transition centered at 556 nm over the course of 1 h (Figure 4). This observation indicated Zn(II)-induced displacement of Co(II) from CP-Ser coordination sphere(s), as anticipated from the Irving–Williams series,[50] and suggested that Co(II) and Zn(II) share the same binding site(s). Moreover, titration of 400 μM CP-Ser with a 1:1 Co:Zn mixture resulted in negligible absorption change at 556 nm (Figure S33), revealing that Zn(II) prevented Co(II)

dx.doi.org/10.1021/ja307974e | J. Am. Chem. Soc. 2012, 134, 18089–18100

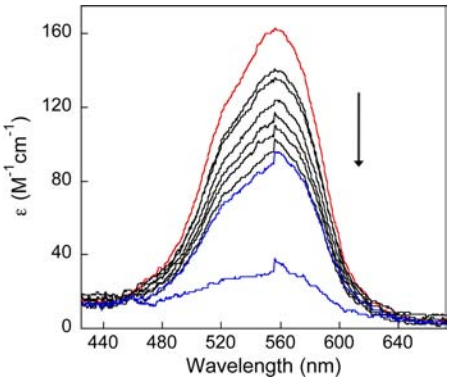

Figure 4. Optical absorption spectra revealing displacement of Co(II) from 100 μM CP-Ser by Zn(II) addition at pH 7.0 (75 mM HEPES, 100 mM NaCl) and T = 25 °C. Red line: Optical absorption spectrum of CP-Ser in the presence of 1 equiv of Co(II). Black lines: Optical absorption spectrum immediately after the addition of 1 equiv of Zn(II) and at t = 15, 30, 45, 60, and 90 min after addition of Zn(II). Blue spectra: Optical absorption spectra immediately (top) and 60 min (bottom) after addition of a second equivalent of Zn(II).

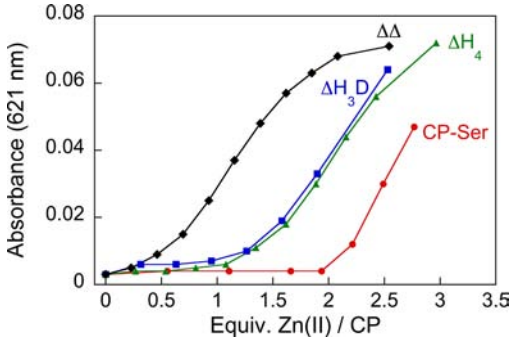

Figure 5. Zinc response of 25 μM Zincon in the presence of ca. 10 μM CP at pH 7.5 (75 mM HEPES, 100 mM NaCl) and 25 °C. The absorption values at 621 nm indicate that Zincon only responds to Zn(II) after CP-Ser binds 2 equiv (red circles) or after ΔHis_4 and ΔHis_3Asp each coordinate 1 equiv of Zn(II) (green triangles and blue squares, respectively). Negligible attenuation of the Zincon response is observed in the presence of ΔΔ (black diamonds).

coordination by CP at least at the His_3Asp site. This set of experiments did not afford conclusive evidence for Zn(II) coordination at the His_4 site because the absorption band corresponding to Co(II) bound to the His_4 site is weak.

Zinc-binding titrations employing CP-Ser or a mutant and a colorimetric Zn(II) indicator were next conducted to ascertain the Zn(II):CP stoichiometries (Figure 5). Titration of a 1:1 mixture of CP-Ser and the low-affinity Zn(II) indicator Zincon ($K_d \approx 10$ μM)[40,41] with Zn(II) afforded a colorimetric response only after >2 equiv of Zn(II) was added, indicating that CP binds two zinc ions with higher affinity than Zincon and supporting formation of a 2:1 Zn:CP complex (75 mM HEPES, 100 mM NaCl, pH 7.5). In contrast, a colorimetric response from Zincon was first observed at ca. 1 equiv of Zn(II) for titrations of 1:1 Zincon and ΔHis_4 or ΔHis_3Asp, confirming that both interfacial sites coordinate Zn(II). Titration of Zincon in the presence of the ΔΔ mutant resulted in negligible perturbation to the Zn(II)-binding curve relative to buffer alone. This mutant does not coordinate Zn(II) to an appreciable extent as previously suggested for ΔZn/Mn from the interpretation of ITC data.[25] In total, the Zincon titrations indicate that CP binds 2 equiv of Zn(II) with K_d values below the low-micromolar range, and with one Zn(II) ion coordinating at the His_3Asp and the second ion at the His_4 site. Judging by the ΔΔ titration, Zincon detected no appreciable Zn(II)-binding to either the His-rich C-terminal tail of A9 or the EF-hand domains of CP. Analogous titrations employing the nanomolar-affinity Zn(II) indicator MF2 ($K_d \approx$ 20 nM)[42,43] also supported a 2:1 Zn:CP complex and indicated that both the ΔHis_3Asp and ΔHis_4 mutants exhibit low nanomolar or greater affinity for Zn(II) (Figure S34).

To further probe Zn(II) binding by heterodimeric CP, a series of Zn(II) competitions were performed by using the turn-on fluorescence Zn(II) sensor FZ3 (K_d = 9 nM).[51] No change in FZ3 emission was observed following addition of 2 μM Zn(II) to a mixture of 2 μM FZ3 and 10 μM CP-Ser (Figure 6). This result was in good agreement with the MF2 titrations and indicated that CP has an apparent dissociation constant for Zn(II) in the sub-nanomolar range. In contrast, ~2- (ΔHis_4) and ~17-fold (ΔHis_3Asp) fluorescence enhancements occurred when the site mutants were mixed with FZ3.

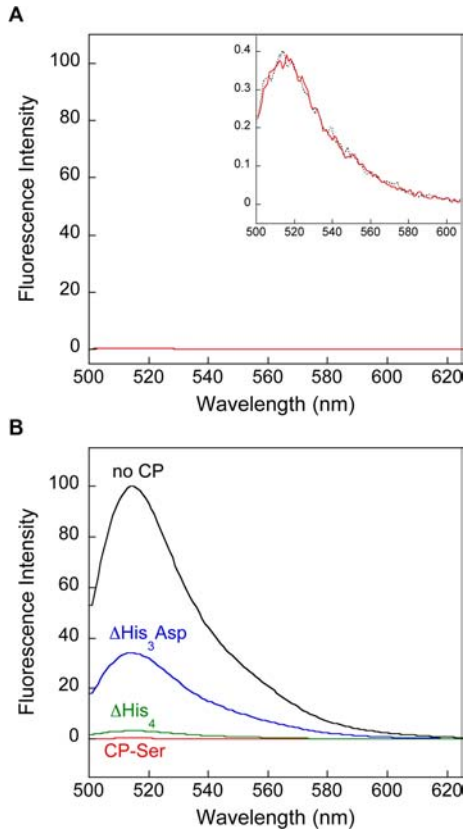

Figure 6. Fluorescence response of 2 μM FZ3 to 2 μM Zn(II) in the presence of 10 μM CP at pH 7.5 (75 mM HEPES, 100 mM NaCl) and 25 °C. (A) No fluorescence change is observed following addition of Zn(II) to mixtures of FZ3 and CP-Ser. Inset: Expansion of the y-axis. Dotted black line, FZ3 emission in the absence of Zn(II); solid red line, FZ3 emission after addition of Zn(II). (B) Fluorescence enhancement is observed for FZ3 in the presence of ΔHis_4 (~2-fold, green line) and ΔHis_3Asp (~17-fold, blue line). FZ3 in the absence of any protein (e.g., no CP, black line) exhibits ~40-fold fluorescence turn-on following addition of 1 equiv of Zn(II). The maximum emission for FZ3 in the presence of 1 equiv of Zn(II) was adjusted to an integrated emission value of 100, and the remaining emission spectra were scaled accordingly.

dx.doi.org/10.1021/ja307974e | J. Am. Chem. Soc. 2012, 134, 18089−18100

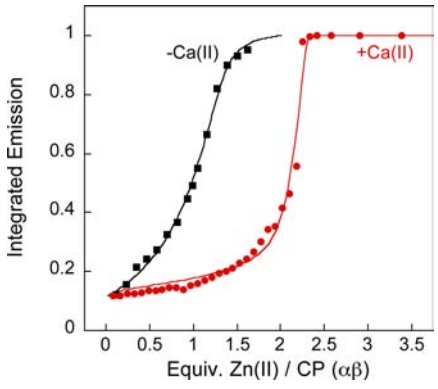

Figure 7. Fluorescence response of 2 μM ZP4 to Zn(II) in the presence of 10 μM CP-Ser at pH 7.5 (75 mM HEPES, 100 mM NaCl) and 25 °C. Each emission spectrum was integrated and the resulting values were normalized to the maximum response and plotted against equivalents of Zn(II) per CP-Ser ($\alpha\beta$). The black squares indicate the titration performed in the absence of Ca(II). The red circles indicate the titration performed in the presence of 200 μM Ca(II). A representative titration for each set of conditions is shown. The titrations were fit to a two binding-site model. The black and red lines represent the fits. The K_d values are K_{d1} = 133 ± 58 (−Ca), ≤10 pM (+Ca) and K_{d2} = 185 ± 219 nM (−Ca), ≤240 pM (+Ca). The K_{d1} and K_{d2} values are assigned to the His_3Asp and His_4 sites, respectively. Excitation was provided at 495 nm, and the emission spectra were integrated from 505 to 650 nm. The corresponding titrations for ΔHis_3Asp and ΔHis_4 are presented in Figure S35.

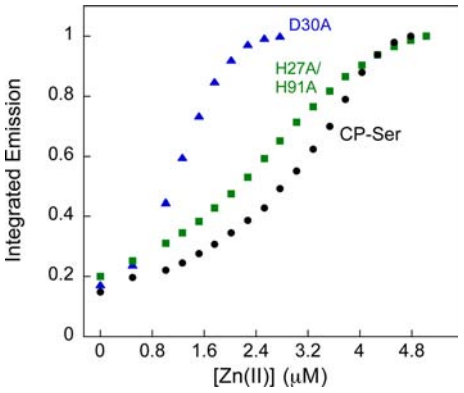

Figure 8. Fluorescence response of 2 μM ZP4 to Zn(II) in the presence of ∼5 μM CP-Ser (black circles), the (A8)H27A/(A9)H91A double mutant (green squares), or the (A8)D30A single mutant (blue triangles). Each emission spectrum was integrated, and the resulting values were normalized to the maximum response. For all titrations, excitation was provided at 495 nm, and the emission spectra were integrated from 505 to 650 nm.

This set of experiments suggested an apparent K_d ordering of CP-Ser < ΔHis_4 < ΔHis_3Asp.

Competition for Zn(II) between CP-Ser ($\alpha\beta$) and ZP4,[44] a Ca(II)-insensitive Zn(II) sensor that forms a 1:1 Zn:ZP4 complex with a dissociation constant of 650 ± 100 pM was observed (Figure 7). In contrast, the ΔHis_4, ΔHis_3Asp, and ΔΔ mutants did not compete with ZP4 for Zn(II) (Figures S35 and S36). Zinc-binding titrations conducted using 10 μM CP-Ser and 2 μM ZP4 were fit to a two-site model, which afforded dissociation constants of K_{d1} = 133 ± 58 pM and K_{d2} = 185 ± 219 nM (Figure 7 and see Supporting Information). Guided by the FZ3 competition results, the picomolar and the nanomolar K_d values were assigned to the His_3Asp and His_4 sites, respectively. Further support for these assignments was obtained from Zn(II) competition titrations performed using ZP4 and CP-Ser single- or double-point mutants (Figure 8). Substitution of CP-Ser for (A8)H27A/(A9)H91A resulted in negligible change to the CP/ZP4/Zn titration curve whereas the Zn(II) competition was attenuated for the (A9)D30A mutant. Based on the MF2 and FZ3 experiments, we contend that the K_{d2} value assigned to the His_4 site is in the lower nanomolar region of the error range obtained from the ZP4 titrations.

Calprotectin Exhibits Calcium-Dependent Affinity for Zn(II) in the Picomolar Range. Zinc-binding titrations employing CP/Zincon mixtures were conducted in the presence of Ca(II) (200 μM $CaCl_2$; 75 mM HEPES, 100 mM NaCl, pH 7.5) to determine whether Ca(II) coordination by CP alters the Zn(II):CP stoichiometry. These titrations afforded 2:1 (CP-Ser) and 1:1 (ΔHis_3Asp and ΔHis_4) Zn:CP($\alpha\beta$) stoichiometries as observed in the absence of Ca(II) (Figure S37).

When 150−450 μM Ca(II) was added to solutions of CP-Ser and ZP4 (75 mM HEPES, 100 mM NaCl, pH 7.5), the Zn(II)-induced fluorescence response of ZP4 was attenuated relative to that observed in the absence of Ca(II) (Figure 7). Enhancement of ZP4 emission occurred only following addition of ∼1.5 equiv of Zn(II) relative to CP-Ser, resulting in a marked shift of the titration curve relative to that obtained in the absence of Ca(II). Moreover, both the ΔHis_3Asp and the ΔHis_4 mutant outcompeted ZP4 for Zn(II) in the presence of 200 μM Ca(II) (Figures S35 and S36). Calcium coordination by the EF-hand domains of CP therefore resulted in increased Zn(II) affinity at both the His_3Asp and His_4 sites. The +Ca(II) titration curves for CP-Ser could be fit with a two-site model using $K_{d1} \leq 10$ pM and $K_{d2} \leq 240$ pM. Because CP outcompetes ZP4 in the presence of Ca(II), these values provide limits on the Zn(II) dissociation constants. The Zn(II) K_d values determined in this work are markedly different from the K_d values reported for wild-type CP obtained by fitting an exothermic event observed by ITC to a two-site model (K_{d1} = 1.4 nM; K_{d2} = 5.6 nM).[25] The discrepancy between the K_d values obtained by fitting the ITC data to a two-site model and the K_d values obtained in this work may be attributed to the limited sensitivity of ITC, which cannot accurately report on picomolar-affinity binding events, as well as different sample conditions. The ITC experiments were conducted in the presence of Tris buffer and millimolar β-mercaptoethanol, both of which form complexes with transition metal ions and therefore impact metal speciation, and in the presence of stoichiometric Ca(II). Based on the current work, this calcium concentration is insufficient to fully tetramerize CP and will complicate analysis of the heterodimer.

The Zn(II) response of ZP4 in the presence of the ΔΔ mutant was comparable to the no-CP control and unaffected by Ca(II) addition (Figures 9A and S36). This experiment provided no evidence for the formation of an additional high-affinity Zn(II)-binding site resulting from Ca(II) complexation.

Next, mixtures of CP and Zn(II)-saturated ZP4 were spiked with 200 μM Ca(II) and the fluorescence change monitored over time. Emission of the Zn(II):ZP4 complex remained constant in the absence of CP and in the presence of non-coordinating ΔΔ, in agreement with expectations based on its slow dissociation rate constant ($k_{off} = 3.4 \times 10^{-3}$ s^{-1}, 25 °C).[52] In contrast, a decrease in Zn(II):ZP4 emission occurred in the presence of CP-Ser, ΔHis_3Asp, and ΔHis_4 over the course of

dx.doi.org/10.1021/ja307974e | J. Am. Chem. Soc. 2012, 134, 18089−18100

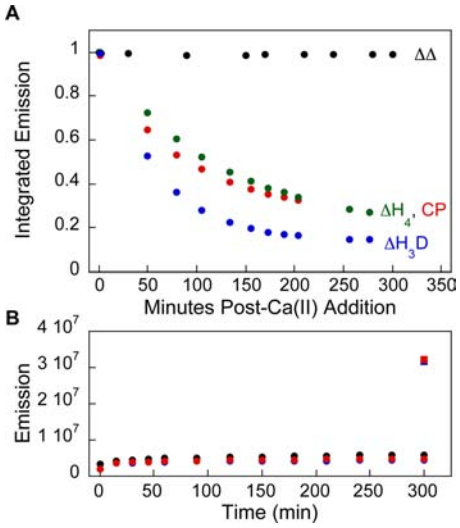

Figure 9. Competition experiments with ZP4 and CP-Ser at pH 7.5 (75 mM HEPES, 100 mM NaCl) and 25 °C. (A) Fluorescence response of 2 μM ZP4 following addition of 200 μM Ca(II) to mixtures of Zn(II):ZP4 and CP. Solutions of ZP4 and CP were titrated with Zn(II) until maximum turn-on of ZP4 was observed (data not shown) and Ca(II) was subsequently added (t = 0 min). Black circles, 10.6 μM ΔΔ; green circles, 9.4 μM ΔHis_4; red circles, 5.8 μM CP-Ser; blue circles, 7.4 μM ΔHis_3Asp. The normalized integrated emission value of 1 corresponds to maximum emission from ZP4. (B) Integrated emission from 1.9 μM ZP4 in the presence of 1:2 Zn(II):CP-Ser. Black circles, ZP4 only; blue circles, ZP4 and CP-Ser; red circles, ZP4 and 1:2 Zn(II):CP-Ser. Addition of 50 μM Zn(II) to the solutions at t = 300 min resulted in ZP4 turn-on as indicated by the data points at $y \approx 3 \times 10^7$. Excitation was provided at 495 nm and the emission spectra were integrated from 500 to 650 nm.

300 min (Figure 9A). This observation is consistent with CP removing Zn(II) from ZP4. Subsequent addition of Zn(II) to these mixtures afforded full turn-on of ZP4 and confirmed that the dye remained Zn(II) responsive during the experiment (data not shown). Both the His_3Asp and His_4 sites of CP can therefore sequester Zn(II) from a picomolar chelator when CP is in its calcium-bound form. Lastly, 2 μM ZP4 was added to solutions containing 1:2 Zn(II):CP with and without 200 μM Ca(II) and the fluorescence of ZP4 monitored over time (Figures 9B and S38). The emission changes observed in the absence and presence of Ca(II) were comparable to those of the apo ZP4 in buffer control over the course of 300 min, suggesting that CP has a slow Zn(II) dissociation rate.

The CD spectrum of 10 μM CP-Ser was unperturbed by the addition of 3 equiv of Zn(II) in both the presence and absence of Ca(II) (Figure S39), revealing that Zn(II) binding to the His_3Asp and His_4 sites has negligible impact on the overall secondary structure of CP-Ser. This observation is in agreement with the CD spectrum of wild-type CP in the presence Zn(II).[45]

Calprotectin Utilizes Calcium To Trigger Antibacterial Action *in vitro*. The growth inhibitory activity of wild-type CP against *S. aureus* ATCC 25923 was first evaluated to confirm the integrity and activity of the recombinant protein (Figures 10 and S40). As expected, negligible growth of *S. aureus* was observed in the presence of 500 μg/mL CP under standard *in vitro* assay conditions and in the presence of a 2 mM Ca(II) supplement.[9,25] Antibacterial activity assays conducted using media lacking the calcium supplement revealed that CP has a slight growth-promoting effect for *S. aureus* ATCC 25923 in the absence of Ca(II) (Figure S40). These observations confirmed that Ca(II) is important for CP-mediated growth inhibition of *S. aureus* ATCC 25923, in agreement with prior observations for *S. aureus* Newman.[9] CP-Ser exhibited calcium-dependent activity comparable to that of the wild-type protein, indicating that neither (A8)Cys42 nor (A9)Cys3 are essential for CP activity (Figures 10 and S40). Calcium-dependent growth inhibition of *E. coli* ATCC 25922 and *E. aerogenes* ATCC 10348 was also observed for CP and CP-Ser (Figure 10). These studies support the notion that CP utilizes calcium to turn on its antibacterial action against Gram-negative and -positive organisms. Moreover, these assays show that the Cys residues of S100A8 and S100A9 are not essential for antibacterial action against several different bacterial species.

Calprotectin Requires at Least One Metal-Binding Site for Antibacterial Activity *in Vitro*. To ascertain whether one or both transition metal-ion binding sites are necessary for CP antibacterial action, *S. aureus*, *E. coli*, and *E. aerogenes* cultures were treated with 500 μg/mL wild-type CP or mutant and monitored at t = 8 and 20 h (Figure 11). The CP mutants all exhibit Cys to Ser mutations and do not require

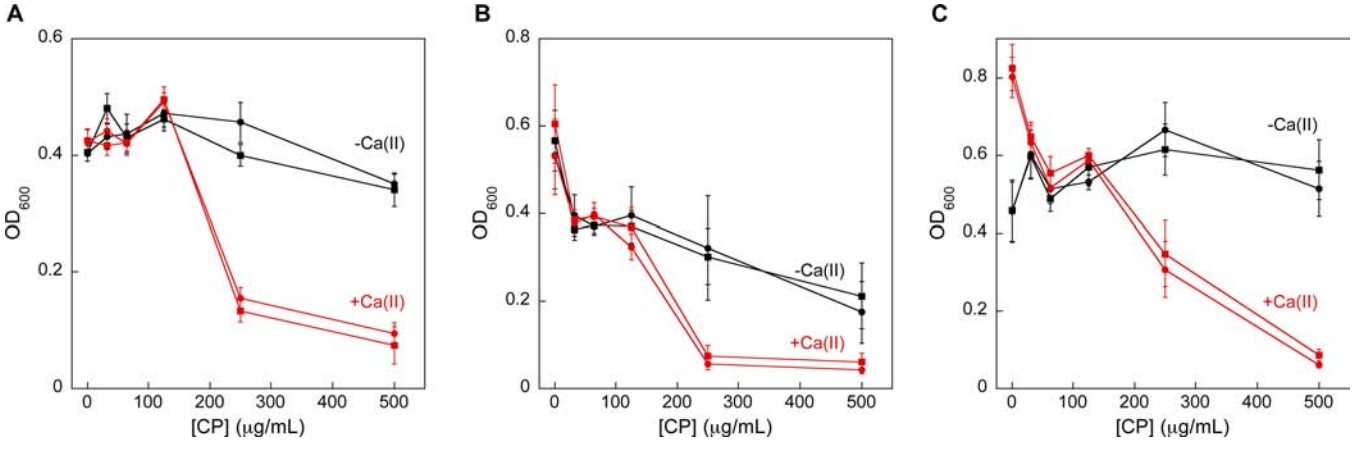

Figure 10. Wild-type CP and CP-Ser exhibit calcium-dependent antibacterial action for both Gram-negative and Gram-positive species. (A) *Enterobacter aerogenes*, (B) *Escherichia coli*, and (C) *Staphylococcus aureus*. The black traces are cultures treated with CP (circles) or CP-Ser (squares) in the absence of a 2 mM Ca(II) supplement. The red traces are for cultures treated with CP (circles) or CP-Ser (squares) in the presence of a 2 mM Ca(II) supplement. The OD_{600} values were recorded at t = 24 h (mean ± SEM for three independent replicates).

dx.doi.org/10.1021/ja307974e | J. Am. Chem. Soc. 2012, 134, 18089−18100

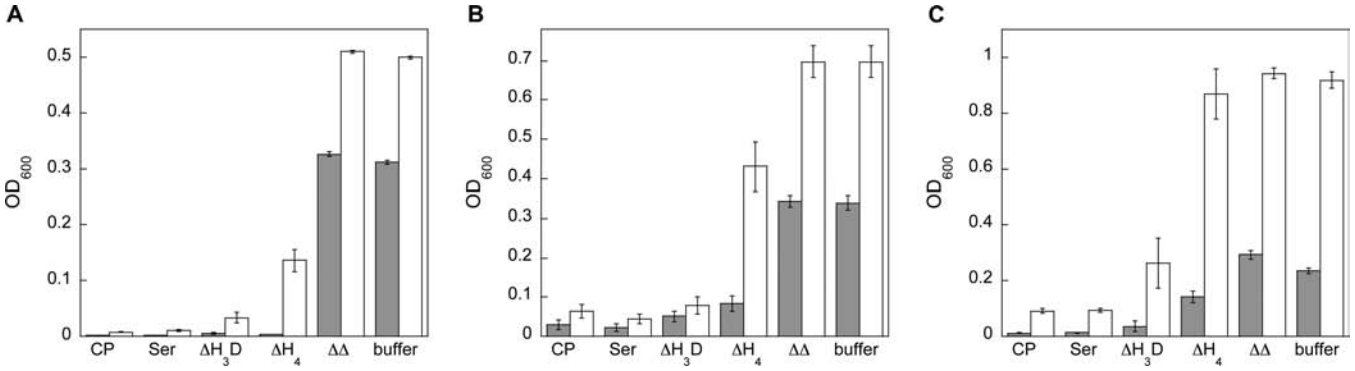

Figure 11. Growth inhibitory activity of 500 μg/mL wild-type CP, CP-Ser, and the metal-binding site mutants. (A) *Enterobacter aerogenes*, (B) *Escherichia coli*, and (C) *Staphylococcus aureus*. The cultures were incubated with 500 μg/mL CP in the presence of a 2 mM Ca(II) supplement (t = 30 °C). The OD_{600} values (mean ± SEM for three independent replicates) were recorded at t = 8 (gray bars) and 20 h (white bars).

reducing agents to prevent protein oxidation, so these assays were conducted in the presence and absence of β-mercaptoethanol (BME), and the +BME results are presented in Figure 11. A synergistic CP/BME effect was observed for *E. coli* at t = 8 h and for all bacterial species at t = 20 h (Figure S41), indicating that BME enhances the activity of CP *in vitro* and independent of the presence of Cys residues. At t = 8 h, both ΔHis_3Asp and ΔHis_4 inhibited the growth of *E. coli* and *E. aerogenes* at levels similar to that of CP/CP-Ser (Figure 11). Although both ΔHis_3Asp and ΔHis_4 inhibited the growth of *S. aureus* relative to the buffer only control, the ΔHis_4 mutant was less effective at inhibiting the growth of this strain. The ΔΔ mutant exhibited no inhibitory effect at 500 μg/mL against *S. aureus*, in accord with prior studies of the ΔZn/Mn mutant reported by others,[25] and also *E. coli* and *E. aerogenes*. At t = 20 h, CP and CP-Ser inhibited the growth of all species, and ΔHis_3Asp and ΔHis_4 inhibited *E. aerogenes* and, to a lesser extent, *E. coli*. In contrast, the *S. aureus* cultures treated with ΔHis_4 exhibited an OD_{600} comparable to that of the buffer-only control. Taken together, one intact metal-binding site is necessary and sufficient for CP growth inhibition of several species *in vitro* on a short ($t \leq 8$ h) time scale. At longer time points, the ΔHis_4 mutant exhibits reduced inhibitory activity, especially for *S. aureus*. The origins of this behavior are currently unclear and may point to an important role of the unusual His_4 site in host defense. It is also possible that the reduced inhibitory activity results from different bacterial physiology or compromised integrity of the ΔHis_4 mutant under the assay conditions.

DISCUSSION

Chelation of zinc and manganese to prevent the uptake and metabolic utilization of these metal nutrients by invading pathogens is one accepted mechanism of action for calprotectin in host defense.[2,3] Nevertheless, precisely how calprotectin coordinates metal ions is largely unexplored, and our current work addresses this important facet of its antimicrobial activity and provides new quantitative and molecular-level insights. The solution studies presented in this work demonstrate that both the His_3Asp and His_4 sites are high-affinity Zn(II)-binding sites and, to the best of our knowledge, provide the first spectroscopic signatures of these sites. The electronic spectra of the cobalt-bound forms indicate that the isolated His_3Asp site houses four- or five-coordinate Co(II), and that the isolated His_4 site likely provides a six-coordinate environment for this metal ion. The summation of the extinction coefficients for cobalt-bound ΔHis_3Asp and ΔHis_4 is smaller in magnitude than the extinction coefficient determined for CP-Ser, which may indicate that metal-ion coordination to one site influences the other. Moreover, the EPR studies presented in this work provide unambiguous signatures for these two distinct Co(II)-binding sites. Further EPR spectroscopic investigations will afford more details about the electronic structures and coordination geometries.[47,49]

The His_4 site exhibited by CP is a very unusual protein-based metal-binding site. The protein data bank contains few examples of first-row transition metals bound to native His_4 sites, which include a manganese-containing photochemical reaction center from *Rhodobacter spaeroides* Y,[53] a manganese-containing cupin from *Thermotoga maritima*,[54] and RemF, a polyketide cyclase from *Streptomyces resistomycificus* crystallized in the zinc-bound form.[55] These structures exhibit six-coordinate M(II) centers. Recent crystallographic studies of S100B revealed pH-dependent ligand swapping and tetrahedral Zn(II) coordination to four His residues at pH 9 whereas the metal ion was coordinated to a His_3Asp motif at lower and higher pH values.[56] Additional spectroscopic and structural investigations are required to ascertain what ligands complete the Co(II) coordination sphere at site 2, and whether this site confers a similar coordination geometry for Zn(II). Zinc adopts four-, five-, and six-coordinate geometries and tetrahedral coordination spheres are most commonly observed in biological systems. A survey of approximately 400 zinc-containing protein structures deposited in the PDB revealed that only 6% of structural Zn(II) sites and 11% of catalytic zinc sites exhibit six-coordinate geometries.[57] Moreover, further evaluation of the His_4 site is necessary to determine whether it confers unique physiological function to CP.

The metal-binding studies presented in this work indicate that the histidine-rich C-terminal extension of S100A9 does not provide an independent Co/Zn-binding site, at least with a K_d value in the micromolar or lower range. Although Zn(II) coordination by the CP EF-hands has been suggested in prior work,[45,58] the Zn(II) competition experiments presented here demonstrate that the EF-hand domains do not complex Zn(II) to an appreciable extent.

Zn(II) competition titrations with CP mutants and the Ca(II)-insensitive Zn(II) sensor ZP4 revealed that calcium binding to the EF-hand domains increases the affinity of CP-Ser for Zn(II) at both the His_3Asp and His_4 sites. Both sites coordinate Zn(II) with sub-nanomolar affinity when CP is in the calcium-bound form. Elucidating the basis for the calcium-

dx.doi.org/10.1021/ja307974e | J. Am. Chem. Soc. 2012, 134, 18089−18100

dependent Zn(II) affinity at the molecular level will require further structural and spectroscopic investigations. In contrast to the canonical EF-hand domain Ca(II)-binding protein calmodulin, S100 family members exhibit subtle conformational changes following Ca(II) complexation.[35] We therefore hypothesize that subtle conformational changes in the Ca(II)-binding loops may organize the Zn(II)-coordination spheres. Indeed, (S100A9)Asp30 of site 1 and (S100A8)His27 of site 2 are components of the Ca(II)-binding loops (Figures 1 and S1).[37]

Extracellular calcium concentrations are in the low-millimolar range, and it is generally accepted that extracellular CP predominantly exists in a Ca(II)-bound form. As a result, the K_d values of ≤10 pM (His_3Asp) and ≤240 pM (His_4), obtained in the presence of Ca(II), indicate the Zn(II) affinity of extracellular CP and are relevant to evaluating a competition between CP and pathogenic microorganisms for Zn(II). The Zn(II) dissociation constants reported for bacterial M(II) transporter proteins typically span the nanomolar range as summarized in Table S9.[59−62] For example, *E. coli* ZnuA is a periplasmic Zn(II) transporter with a reported K_d value of <20 nM for this metal ion.[59] The metal transporter PsaA of *Streptococcus pneumoniae* was recently shown to coordinate Zn(II) with $K_d \approx 230$ nM.[60] The sub-nanomolar Zn(II) dissociation constants reported in this work indicate that CP ($\alpha_2\beta_2$) outcompetes such transporters for Zn(II), providing quantitative insight into the antibacterial activity of CP attributed to Zn(II) sequestration. Nevertheless, whether the antibacterial activity of calprotectin results solely from chelating free zinc at sites of infection is an important question. CP ($\alpha_2\beta_2$) removes Zn(II) from the picomolar-affinity chelator ZP4, and it may also inhibit zinc-binding proteins, such as extracellular zinc proteases utilized by pathogens,[63] via Zn(II) chelation. A series of *in vitro* assays reported in the medical literature indicated that CP inhibits human matrix metalloproteinases.[64]

The data presented in this work support the notion that CP primarily exists in a lower Zn(II)-affinity form in the cytoplasm where calcium ion concentrations are generally in the nanomolar range, and that it oligomerizes to a higher Zn(II)-affinity form in the extracellular space where calcium levels are at low millimolar levels. The strategy of using calcium binding to trigger higher-affinity Zn(II) complexation may have several ramifications. It provides an explanation for the calcium-dependent growth inhibition of CP observed *in vitro*. In addition, we propose that calcium-induced switching is important for cytosolic metal-ion homeostasis in the neutrophil. In eukaryotic cells, total intracellular zinc concentrations are in the micromolar range, and most of this Zn(II) is bound in high-affinity protein sites.[65] The resulting cytoplasmic free zinc concentrations are estimated to fluctuate in the picomolar range based on recent measurements in a variety of eukaryotic cell types.[65−68] Storing cytoplasmic CP in the heterodimeric ($\alpha\beta$) form may prevent unwanted Zn(II) sequestration in the cytosol. Along these lines, how CP contributes to transition metal ion homeostasis in the cytoplasm of neutrophils and other cell types, and whether calcium signaling plays a role, is unclear and warrants careful examination.

Further evaluation of the interplay between Zn(II) and CP beyond infectious disease is also important. Both CP and Zn(II) have immunomodulatory functions. Calprotectin is a major component of corpora amylacea inclusions in the diseased prostate, which have abundant calcium and zinc.[32] Moreover, zinc dysregulation plays a role in cancer progression, and this metal may contribute to the mechanisms of CP in carcinogenesis.[30,31] Lastly, hypercalprotectinanemia is a rare disease of erroneous Zn(II) metabolism characterized by anemia, inflammation, recurrent infections, and hyperzincanemia.[33,34] Patients present >1000-fold elevated levels of plasma CP and high plasma zinc concentrations, indicating excessive zinc-bound CP in circulation and Zn(II) depletion from tissues. Taking these clinical observations together, molecular-level understanding of how CP and Zn(II) contribute to the pathophysiology of various human diseases is necessary and may provide new insights into therapeutic development.

In closing, calprotectin is clearly a multifaceted protein influencing both microbial and mammalian physiology. Zinc sequestration by calprotectin in the context of infection is only one layer of its many appreciated, and also underappreciated, contributions to the biology and homeostasis of transition metal ions, the details of which will be further unveiled through concerted efforts at the molecular, cellular, and organismal levels.

■ ASSOCIATED CONTENT

Supporting Information

Complete ref 54, supporting experimental methods, design of the synthetic genes, custom DynaFit script, Tables S1−S9, and Figures S1−S42; Figure S42 contains the chemical structures of all Zn(II) indicators used in this work. This material is available free of charge via the Internet at http://pubs.acs.org.

■ AUTHOR INFORMATION

Corresponding Author

lnolan@mit.edu

Notes

The authors declare no competing financial interest.

■ ACKNOWLEDGMENTS

We acknowledge the Office of the Director, National Institutes of Health (NIH Grant DP2OD007045), the Searle Scholars Program (Kinship Foundation), the Center for Environmental Sciences at MIT (NIH Grant P30-ES002109), and the Department of Chemistry at MIT for financial support. We thank Profs. Walter Chazin and Eric Skaar, and members of their laboratories, for graciously sharing expertise on the purification and handling of calprotectin. We thank Dr. Jeff Simpson for assistance with the EPR spectrometer, Ms. Debbie Pheasant for assistance with the CD spectrometer, Dr. Petr Kuzmic for guidance with DynaFit, and Ms. Jingnan Lu, Ms. Yuxin Xie, Ms. Sumin Kim, and Ms. Lisa Cunden for assistance with the subcloning and protein purifications. EPR spectroscopic instrumentation is maintained by the MIT Department of Chemistry Instrumentation Facility. The MIT Biophysical Instrumentation Facility for the Study of Complex Macromolecular Systems, which is supported by grants NSF-0070319 and NIH GM68762, maintains the circular dichroism spectrophotometer.

■ REFERENCES

(1) Weinberg, E. D. *JAMA* **1975**, *231*, 39−341.
(2) Kehl-Fie, T. E.; Skaar, E. P. *Curr. Opin. Chem. Biol.* **2009**, *14*, 218−224.
(3) Hood, M. I.; Skaar, E. P. *Nat. Rev. Microbiol.* **2012**, *10*, 525−537.
(4) Johnson, E. E.; Wessling-Resnick, M. *Microbes Infect.* **2012**, *14*, 207−216.

(5) Weinberg, E. D. *Biochim. Biophys. Acta* **2009**, *1790*, 600−605.
(6) Vallee, B. L.; Falchuk, K. H. *Physiol. Rev.* **1993**, *73*, 79−118.
(7) Papp-Wallace, K. M.; Maguire, M. E. *Annu. Rev. Microbiol.* **2006**, *60*, 187−209.
(8) Sohnle, P. G.; Collins-Lech, C.; Wiessner, J. H. *J. Infect. Dis.* **1991**, *164*, 137−142.
(9) Corbin, B. D.; Seeley, E. H.; Raab, A.; Feldmann, J.; Miller, M. R.; Torres, V. J.; Anderson, K. L.; Dattilo, B. M.; Dunman, P. M.; Gerads, R.; Caprioli, R. M.; Nacken, W.; Chazin, W. J.; Skaar, E. P. *Science* **2008**, *319*, 962−965.
(10) Hunter, M. J.; Chazin, W. J. *J. Biol. Chem.* **1998**, *273*, 12427−12435.
(11) Leukert, N.; Sorg, C.; Roth, J. *J. Biol. Chem.* **2005**, *386*, 429−434.
(12) Leukert, N.; Vogl, T.; Strupat, K.; Reichelt, R.; Sorg, C.; Roth, J. *J. Mol. Biol.* **2006**, *359*, 961−972.
(13) Vogl, T.; Roth, J.; Sorg, C.; Hillenkamp, F.; Strupat, K. *J. Am. Soc. Mass Spectrom.* **1999**, *10*, 1124−1130.
(14) Strupat, K.; Rogniaux, H.; Van Dorsselaer, A.; Roth, J.; Vogl, T. *J. Am. Soc. Mass Spectrom.* **2000**, *11*, 780−788.
(15) Nathan, C. *Nat. Rev. Immunol.* **2006**, *6*, 173−182.
(16) Johne, B.; Fagerhol, M. K.; Lyberg, T.; Prydz, H.; Brandtzaeg, P.; Naess-Andresen, C. F.; Dale, I. *J. Clin. Pathol: Mol. Pathol.* **1997**, *50*, 113−123.
(17) Brinkmann, V.; Zychlinsky, A. *Nat. Rev. Microbiol.* **2007**, *5*, 577−582.
(18) Urban, C. F.; Ermert, D.; Schmid, M.; Abu-Abed, U.; Goosmann, C.; Nacken, W.; Brinkmann, V.; Jungblut, P. R.; Zychlinsky, A. *PloS Pathog.* **2009**, *5*, e1000639.
(19) Bianchi, M.; Niemiec, M. J.; Siler, U.; Urban, C. F.; Reichenbach, J. *J. Allergy Clin. Immunol.* **2011**, *127*, 1243−1252.
(20) McCormick, A.; Heesemann, L.; Wagener, J.; Marcos, V.; Hartl, D.; Loeffler, J.; Heesemann, J.; Ebel, F. *Microbes Infect.* **2010**, *12*, 928−936.
(21) Liu, J. Z.; Jellbauer, S.; Poe, A. J.; Ton, V.; Pesciaroli, M.; Kehl-Fie, T. E.; Restrepo, N. A.; Hosking, M. P.; Edwards, R. A.; Battistoni, A.; Pasquali, P.; Lane, T. E.; Chazin, W. J.; Vogl, T.; Roth, J.; Skaar, E. P.; Raffatellu, M. *Cell Host Microbe* **2012**, *11*, 227−239.
(22) Steinbakk, M.; Naess-Andresen, C. F.; Lingaas, E.; Dale, I.; Brandtzaeg, P.; Fagerhol, M. K. *Lancet* **1990**, *336*, 763−765.
(23) Zaia, A. A.; Sappington, K. J.; Nisapakultorn, K.; Chazin, W. J.; Dietrich, E. A.; Ross, K. F.; Herzberg, M. C. *Mucosal Immunol.* **2009**, *2*, 43−53.
(24) Lusitani, D.; Malawista, S. E.; Montgomery, R. R. *Infect. Immun.* **2003**, *71*, 4711−4716.
(25) Kehl-Fie, T. E.; Chitayat, S.; Hood, M. I.; Damo, S.; Restrepo, N.; Garcia, C.; Munro, K. A.; Chazin, W. J.; Skaar, E. P. *Cell Host Microbe* **2011**, *10*, 158−164.
(26) Loomans, H. J.; Hahn, B. L.; Li, Q.-Q.; Phadnis, S. H.; Sohnle, P. G. *J. Infect. Dis.* **1998**, *177*, 812−814.
(27) Clohessy, P. A.; Golden, B. E. *Scand. J. Immunol.* **1995**, *42*, 551−556.
(28) Sohnle, P. G.; Hunter, M. J.; Hahn, B.; Chazin, W. J. *J. Infect. Dis.* **2000**, *182*, 1272−1275.
(29) Russell, D. G. *Cell Host Microbe* **2008**, *3*, 115−116.
(30) Nakatani, Y.; Yamazaki, M.; Chazin, W. J.; Yui, S. *Mediators Inflamm.* **2005**, *5*, 280−292.
(31) Wan, S.-G.; Taccioli, C.; Jiang, Y. B.; Chen, H. P.; Smalley, K. J.; Huang, K.; Liu, X.-P.; Farber, J. L.; Croce, C. M.; Fong, L. Y. Y. *Int. J. Cancer* **2011**, *129*, 331−345.
(32) Yanamandra, K.; Alexeyev, O.; Zamotin, V.; Srivastava, V.; Shchukarev, A.; Brorsson, A. C.; Tartaglia, G. G.; Vogl, T.; Kayed, R.; Wingsle, G.; Olsson, J.; Dobson, C. M.; Bergh, A.; Elgh, F.; Morozova-Roche, L. A. *PLoS One* **2009**, *4*, e5562.
(33) Gustafsson, D.; Breimer, L. H.; Isaksson, H. S.; Nilsson, T. K. *Scand. J. Clin. Lab. Invest.* **2012**, *72*, 34−38.
(34) Sampson, B.; Fagerhol, M. K.; Sunderkötter, C.; Golden, B. E.; Richmond, P.; Klein, N.; Kovar, I. Z.; Beattie, J. H.; Wolska-Kusnierz, B.; Saito, Y.; Roth, J. *Lancet* **2002**, *360*, 1742−1745.
(35) Gifford, J. L.; Walsh, M. P.; Vogel, H. J. *Biochem. J.* **2007**, *405*, 199−221.
(36) Chazin, W. J. *Acc. Chem. Res.* **2011**, *44*, 171−179.
(37) Korndörfer, I. P.; Brueckner, F.; Skerra, A. *J. Mol. Biol.* **2007**, *370*, 887−898.
(38) Brodersen, D. E.; Nyborg, J.; Kjeldgaard, M. *Biochemistry* **1999**, *38*, 1695−1704.
(39) Moroz, O. V.; Blagova, E. V.; Wilkinson, A. J.; Wilson, K. S.; Bronstein, I. B. *J. Mol. Biol.* **2009**, *391*, 536−551.
(40) Maret, W.; Vallee, B. L. *Proc. Natl. Acad. Sci. U.S.A.* **1998**, *95*, 3478−3482.
(41) Talmard, C.; Bouzan, A.; Faller, P. *Biochemistry* **2007**, *46*, 13658−13666.
(42) Simons, T. J. B. *J. Biochem. Biophys. Methods* **1993**, *27*, 25−37.
(43) Golynskiy, M. V.; Gunderson, W. A.; Hendrich, M. P.; Cohen, S. M. *Biochemistry* **2006**, *45*, 15359−15372.
(44) Burdette, S. C.; Frederickson, C. J.; Bu, W.; Lippard, S. J. *J. Am. Chem. Soc.* **2003**, *125*, 1778−1787.
(45) Vogl, T.; Leukert, N.; Barczyk, K.; Strupat, K.; Roth, J. *Biochim. Biophys. Acta* **2006**, *1763*, 1298−1306.
(46) Bertini, I.; Luchinat, C. *Adv. Inorg. Biochem.* **1984**, *6*, 71−111.
(47) Bennet, B. *Metals Biol.: Biol. Magn. Reson.* **2010**, *29*, 345−370.
(48) Fielding, A. J.; Kovaleva, E. G.; Farquhar, E. R.; Lipscomb, J. D.; Que, L., Jr. *J. Biol. Inorg. Chem.* **2011**, *16*, 341−355.
(49) Crawford, P. A.; Yang, K.-W.; Sharma, N.; Bennett, B.; Crowder, M. W. *Biochemistry* **2005**, *44*, 5168−5176.
(50) Irving, I.; Williams, R. J. P. *Nature* **1948**, *162*, 746−747.
(51) Krężel, A.; Maret, W. *J. Am. Chem. Soc.* **2007**, *129*, 10911−10921.
(52) Nolan, E. M.; Jaworski, J.; Okamoto, K.-I.; Hayashi, Y.; Sheng, M.; Lippard, S. J. *J. Am. Chem. Soc.* **2005**, *127*, 16812−16823.
(53) Arnoux, B.; Gaucher, J.-F.; Ducruix, A.; Reiss-Husson, F. *Acta Crystallogr. D: Biol. Crystallogr.* **1995**, *51*, 368−379.
(54) Jaroszewski, L.; et al. *Proteins* **2004**, *56*, 611−614.
(55) Silvennoinen, L.; Sandalova, T.; Schneider, G. *FEBS Lett.* **2009**, *583*, 2917−2921.
(56) Ostendorp, T.; Diez, J.; Heizmann, C. W.; Fritz, G. *Biochim. Biophys. Acta* **2011**, *1813*, 1083−1091.
(57) Patel, K.; Kumar, A.; Durani, S. *Biochim. Biophys. Acta* **2007**, *1774*, 1247−1253.
(58) Vogl, T.; Gharibyan, A. L.; Morozova-Roche, L. A. *Int. J. Mol. Sci.* **2012**, *13*, 2893−2917.
(59) Yatsunyk, L. A.; Easton, J. A.; Kim, L. R.; Sugarbaker, S. A.; Bennett, B.; Breece, R. M.; Vorontsov, I. I.; Tierney, D. L.; Crowder, M. W.; Rosenzweig, A. C. *J. Biol. Inorg. Chem.* **2008**, *13*, 271−288.
(60) McDevitt, C. A.; Ogunniyi, A. D.; Valkov, E.; Lawrence, M. C.; Kobe, B.; McEwan, A. G.; Paton, J. C. *PloS Pathog.* **2011**, *7*, e1002357.
(61) Zheng, B.; Zhang, Q. M.; Gao, J.; Han, H.; Li, M.; Zhang, J.; Qi, J.; Yan, J.; Gao, G. F. *PLoS One* **2011**, *6*, e19510.
(62) Desrosiers, D. C.; Bearden, S. W.; Mier, I.; Abney, J.; Paulley, J. T.; Fetherston, J. D.; Salazar, J. C.; Radolf, J. D.; Perry, R. D. *Infect. Immun.* **2010**, *78*, 5163−5177.
(63) Häse, C. C.; Finkelstein, R. A. *Microbiol. Rev.* **1993**, *57*, 823−837.
(64) Isaksen, B.; Fagerhol, M. K. *J. Clin. Pathol.: Mol. Pathol.* **2001**, *54*, 289−292.
(65) Colvin, R. A.; Holmes, W. R.; Fontaine, C. P.; Maret, W. *Metallomics* **2010**, *2*, 306−317.
(66) Krężel, A.; Maret, W. *J. Biol. Inorg. Chem.* **2006**, *11*, 1049−1062.
(67) Bozym, R. A.; Thompson, R. B.; Stoddard, A. K.; Fierke, C. A. *ACS Chem. Biol.* **2006**, *1*, 103−111.
(68) Vinkenborg, J. L.; Nicolson, T. J.; Bellomo, E. A.; Koay, M. S.; Rutter, G. A.; Merkx, M. *Nat. Methods* **2009**, *6*, 737−740.